ACS OMEGA

Article

http://pubs.acs.org/journal/acsodf

Development of Graphene Oxide-/Galactitol Polyester-Based Biodegradable Composites for Biomedical Applications

Janeni Natarajan,[†] Giridhar Madras,[‡] and Kaushik Chatterjee*[,§]

[†]Centre for Nano Science and Engineering, [‡]Department of Chemical Engineering, and [§]Department of Materials Engineering, Indian Institute of Science, C.V. Raman Avenue, Bangalore 560012, India

ABSTRACT: We have developed nanocomposites based on galactitol/adipic acid in the molar ratio of 1:1 with different weight percentages of graphene oxide (GO). The objective of this study was to analyze the effect of enhanced physicochemical properties achieved due to the addition of GO to the polymers on cellular responses. The chemical structures of the polymer and composites were confirmed by Fourier transform infrared spectroscopy. Scanning electron microscopy revealed the uniform distribution of GO in the polymers. Differential scanning calorimetry showed no significant variation in the glass-transition temperature of the nanocomposites. Dynamic mechanical analysis demonstrated the increase of Young's modulus with the increase in the addition of GO to the polymer from 0.5 to 1 wt % and a dramatic decrease in modulus with the addition of 2 wt % GO to the polyester. Contact angle analysis illustrated a slight increase in hydrophilicity with the addition of GO to the polyester. Investigations on the hydrolytic degradation and dye release were performed and revealed that the degradation and release decreased with the increase in the weight percentages of GO but increased for 2 wt % GO with the polymer. The rates of degradation and dye release followed first-order and Higuchi kinetics, respectively. The initial in vitro cytocompatibility studies exhibited minimal toxicity. Mineralization studies proved that these nanocomposites stimulated osteogenesis. This study has salient implications for designing biodegradable polymers for use as scaffolds with tailored release.

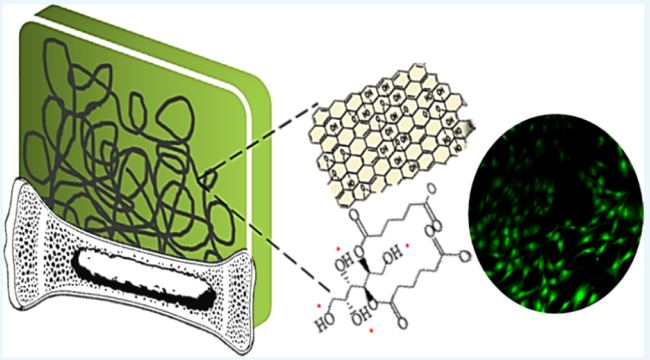

1. INTRODUCTION

The usage of graphene as fillers in polymer nanocomposites has been trending in the recent years owing to its remarkable thermal, mechanical, and electrical properties.[1] Recently, polymer nanocomposites based on graphene were explored in the field of pharmaceutics and tissue regeneration.[2] The mechanical strength of soft polymers can be increased by the incorporation of graphene for potential use in hard tissue engineering applications.[3] Graphene-based nanomaterials were proven to exhibit better cell adhesion, proliferation, and differentiation that could be attributed to its flexibility and adaptability.[4] Because of its noncovalent binding abilities, graphene can play a crucial role in directing the undifferentiated stem cells toward osteogenic lineage.[5]

Robust interfacial interactions between the polymer matrix and the nanoparticle are considered critical in engineering a mechanically strong composite. One popular strategy to achieve good interaction is by chemical functionalization of the surface.[6] The chemical modifications such as addition of hydroxyl and amine groups to the surface of nanoparticles demonstrated better biological responses.[3,7] Graphene oxide (GO), a form of graphene rich in epoxide, carboxyl, and hydroxyl groups, has been explored for biological applications. Despite the nonbiodegradability of graphene, the biocompatibility of graphene is greatly enhanced by synthesizing GO, which is a result of functionalization of graphene.[8] Given the recent surge in studies based on GO nanocomposites, there are numerous reports evaluating their toxicity. When GO is incorporated in polymers in small amounts (<3 wt %), it does not pose any toxicity against mammalian cells.[9] This study showed that GO showed greater cytocompatibility than polymer and there was no statistical difference between the % cytotoxicity of the GO−polymer composite and the polymer. The biocompatibility of GO nanoparticles was well-illustrated for their application in drug delivery.[10] The active chemical groups present in GO were shown to augment interactions with proteins, resulting in improved cell adhesion and proliferation.[5] GO has also been shown to enhance the differentiation of adipose-derived mesenchymal stem cells to osteoblasts.[11]

Polyesters are a widely preferred class of polymers for biomedical applications owing to their innumerable advantages, such as hydrolytic degradation.[12] Thermoset polymers are advantageous for biomedical applications owing to their unaltered structure throughout the degradation as they degrade via a combination of bulk and surface erosion mechanisms.[13] Toxicity can be minimized by choosing monomers based on plant or animal origin that are likely to be cytocompatible. Galactitol, derived from galactose and dicarboxylic acids, is

Received: August 5, 2017
Accepted: August 22, 2017
Published: September 7, 2017

DOI: 10.1021/acsomega.7b01139
ACS Omega 2017, 2, 5545−5556

Scheme 1. Plausible Reaction Scheme for the Synthesis of the Galactitol/Adipic Acid Polyester in the Ratio of 1:1[a]

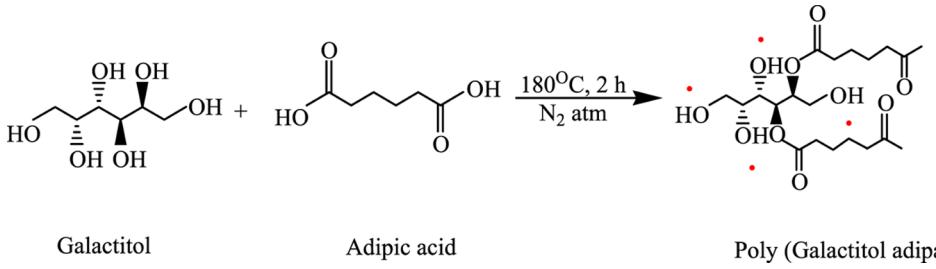

[a]Red dots indicate that these −OH groups might also be involved in esterification because it is a random polymerization.

eliminated via urine and the β-oxidation pathway and thus proven to be less toxic.[14,15]

GO−polymer nanocomposites had been assessed for bone regeneration in the previous reports.[16,17] These reports had demonstrated the contribution of graphene in increasing the mechanical strength and for differentiation of stem cells toward osteogenic lineage. The toxicity of GO is highly size- and dose-dependent, and no toxicity was observed in mice for medium and low doses of GO.[18] The ability of macrophages to engulf GO sheets of about 1 μm has been demonstrated in a previous report.[19] Galactitol and adipic acid, a dicarboxylic acid-based polyester, in the molar ratio of 1:1 was synthesized in this study based on our previous report.[20] Galactitol-based polymers showed good cytocompatibility and potential for bone regeneration. This polymer was chosen based on its lowest modulus (0.37 MPa) among the other polymers synthesized in the study. It was hypothesized that the modulus of this polymer can be increased significantly by the addition of GO for its potential use in bone regeneration. The physical properties, degradation, and release of dyes from the composites have been investigated for different weight percentages of GO in the polymer. To examine their efficiency in inducing osteogenesis, mineralization studies were also conducted.

2. RESULTS AND DISCUSSION

2.1. Polymer Synthesis. The formation of poly(galactitol adipate) (PGaAd) is through the conventional esterification reaction, leading to the ester bond formation with the elimination of water molecules (Scheme 1). The prepolymers were completely soluble in *N*,*N*-dimethylformamide (DMF) and dimethyl sulfoxide (DMSO). After the curing process, the cured polymers do not dissolve in any solvent. The Hummers method used for the preparation of GO is a simple method that eliminates the use of catalyst unlike chemical vapor deposition. Metallic catalysts used in the preparation of GO might be toxic to cells.[21]

The polymers were given the nomenclature based on the first letters of monomers. P corresponds to polymer, Ga denotes galactitol, Ad stands for adipic acid, and GO signifies graphene oxide. The weight percentages of GO added will be indicated in the end. PGaAd stands for poly(galactitol adipate), which is the neat polymer. With the addition of GO, the polymers were denoted PGaAdGO0.5, PGaAdGO1, and PGaAdGO2 for all of the weight percentages of GO used, respectively.

2.2. Polymer Characterization. *2.2.1. Fourier Transform Infrared (FTIR) Spectroscopy.* FTIR spectra[22] (Figure 1) of PGaAd and all composites displayed a characteristic ester carbonyl (C═O) stretching peak around 1720 cm^{-1}. Other peaks such as −OH stretching peaks at 3400 cm^{-1} and asymmetric and symmetric −CH stretching peaks at 2945 and

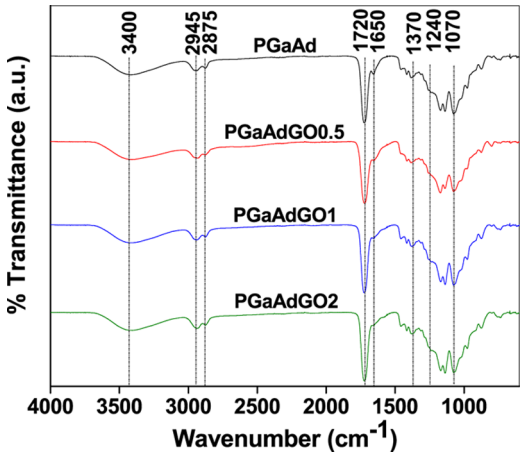

Figure 1. FTIR spectra of PGaAd and composites.

2875 cm^{-1} can be observed in all spectra. The peaks corresponding to the C═C vibration of graphitic domains are visible around 1650 cm^{-1}. The peaks related to carboxyl, carbonyl, and epoxy groups in graphene oxide can be seen at 1370, 1240, and 1070 cm^{-1}, respectively.[23] These peaks are also visible in PGA spectra as the polymer also contains the aforementioned groups.

2.2.2. Proton Nuclear Magnetic Resonance (^{1}H NMR) Spectroscopy. Proton nuclear magnetic resonance (^{1}H NMR) spectroscopy was performed for further verification of the FTIR data of PGaAd (Figure 2). The peaks reported matched with those in the previously reported similar studies.[24] The peaks present between 3.3 and 5.5 ppm could be attributed to the protons of galactitol. The peaks in the regions of 2−3 ppm could be assigned to the protons adjacent to the −COOH groups of adipic acid (HOOC−C**H**$_2$). The peak at 1.5 ppm could be attributed to the protons of −CH$_2$ present next to the −CH$_2$ group in adipic acid (HOOC−CH$_2$−C**H**$_2$).

2.2.3. Differential Scanning Calorimetry (DSC). DSC results demonstrated (Table 1) that T_g increased with an increase in the GO content. This could be attributed to the interfacial interactions between the polymer and the nanofiller.[25] It was also evident from FTIR that the −OH groups and carboxyl groups present in GO interacted with the −OH and −COOH groups of adipic acid during the curing process. This was evident when all of the peaks were normalized to the peak at 1073 cm^{-1} and the areas of the peaks of the composites at 1720 cm^{-1} were greater than those of PGA. Thermal curing of the polymers resulted in the formation of strong covalent bonds and leads to the restriction in polymer chain mobility.[26] Therefore, T_g increases with an increase in the nanofiller content. Many literature reports have shown at least 4 °C

DOI: 10.1021/acsomega.7b01139
ACS Omega 2017, 2, 5545−5556

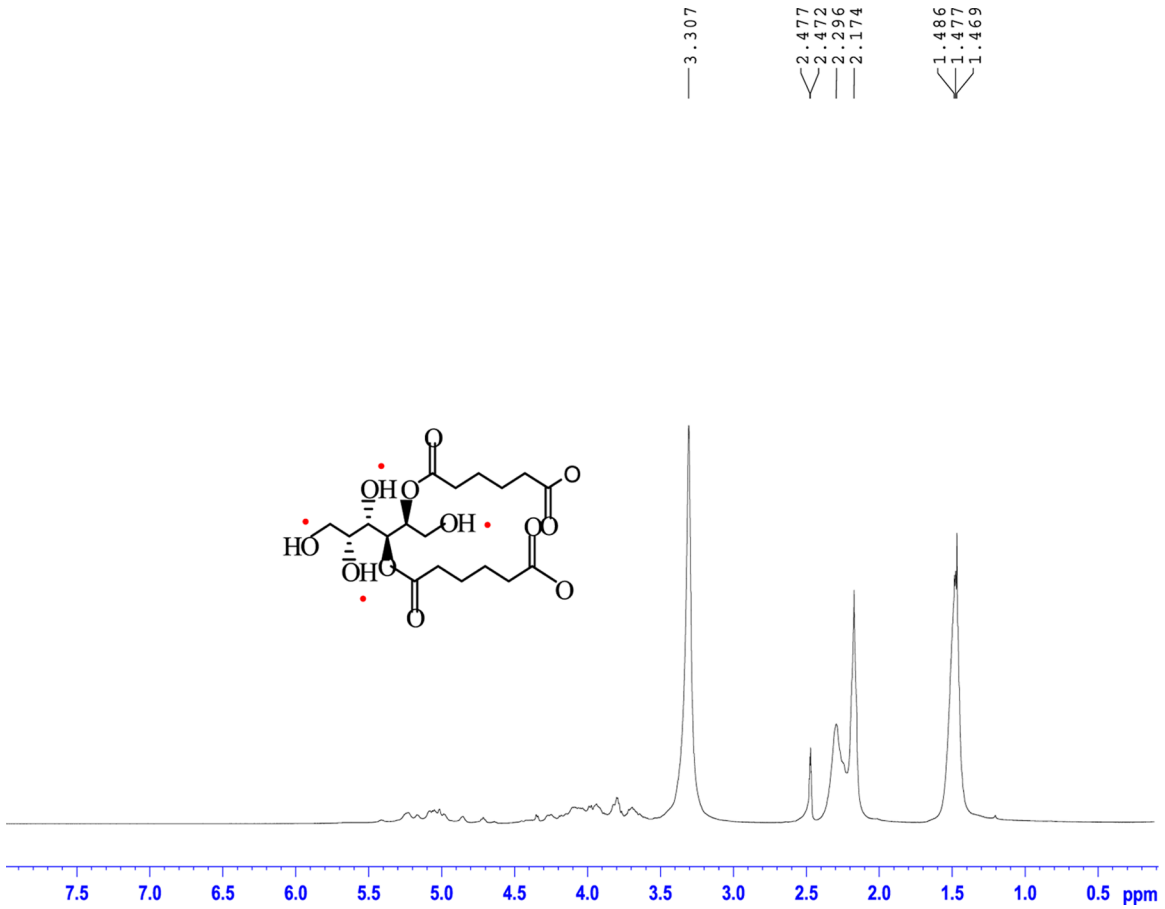

Figure 2. NMR spectra of the prepolymer of PGaAd.

Table 1. Physical Properties, Degradation, and Release Rate Coefficients of PGaAd and Composites

polymers	T_g (±2 °C)	Young's modulus (MPa) at 10 Hz	cross-link density, n (mol/m^3)	contact angle (deg)	degradation rate coefficient, k_d ($\times 10^{-3}$ h^{-1})	rhodamine B (RB) release, k_{RB} ($\times 10^{-3}$ h^{-n})	rhodamine B base (RBB) release, k_{RBB} ($\times 10^{-3}$ h^{-n})
PGaAd	25	0.45	0.00006	82 ± 2	39.1	77.1	75.7
PGaAdGO0.5	27	4.7	0.00061	80 ± 2	22.5	65	62.1
PGaAdGO1	28	33.2	0.00429	78 ± 1	9.7	50.1	48.6
PGaAdGO2	29	6.3	0.00081	75 ± 2	11.1	44.6	39

increase in T_g with the addition of nanofillers, which is similar to that reported in this study, where T_g increased from 25 to 29 °C with the addition of 2 wt % GO to PGaAd.[25] For example, GO intercalated by surfactant was blended with polypropylene-*graft*-maleic anhydride and showed 1.2 °C increase in T_g.[27]

2.2.4. Matrix-Assisted Laser Desorption Ionization Time-of-Flight Mass Spectrometry (MALDI-TOF MS). The molecular weight of the prepolymer of PGaAd was around 973 g/mol (Figure 3), which was similar to the one reported for the other prepolymers in the family of galactitol-based polyesters.[20]

2.2.5. Dynamic Mechanical Analysis (DMA). The mechanical properties investigated using DMA yielded the storage and loss modulus values. Young's modulus was calculated using the storage modulus and loss modulus obtained from DMA using the following formula[28]

$$E^* = \sqrt{E'^2 + E''^2} \quad (1)$$

In eq 1, E^* is the complex modulus, E' is the storage modulus, and E'' refers to the loss modulus. The complex modulus may be approximately considered as Young's modulus. DMA results (Table 1) illustrated the increase in moduli of the composites with an increase in GO reinforcement in polymers for 0.5 and 1 wt %. The moduli decreased with 2 wt % GO content. The moduli increased from 0.45 to 33 MPa with the addition of 1 wt % GO to PGaAd and then decreased to 6 MPa with the addition of 2 wt % GO. The increase in moduli values could be due to the transfer of stress from a soft polymer matrix to hard fillers.[29] The small increase could be due to the structural defects of graphene sheets.[30] The decrease in the modulus values could be ascribed to the possibility of agglomeration and nonuniformity in dispersion with an increase in the filler loading. A similar decrease has been reported for GO, carbon nanotubes, and other carbonaceous filler materials.[31,32] In a similar study, the modulus increased from 209 to 305 MPa when poly(ϵ-caprolactone) (PCL) and 1% GO were blended.[33]

On the basis of the values of the calculated complex modulus, the cross-linking densities for PGaAd and composites were calculated using the following formula[15]

DOI: 10.1021/acsomega.7b01139
ACS Omega 2017, 2, 5545−5556

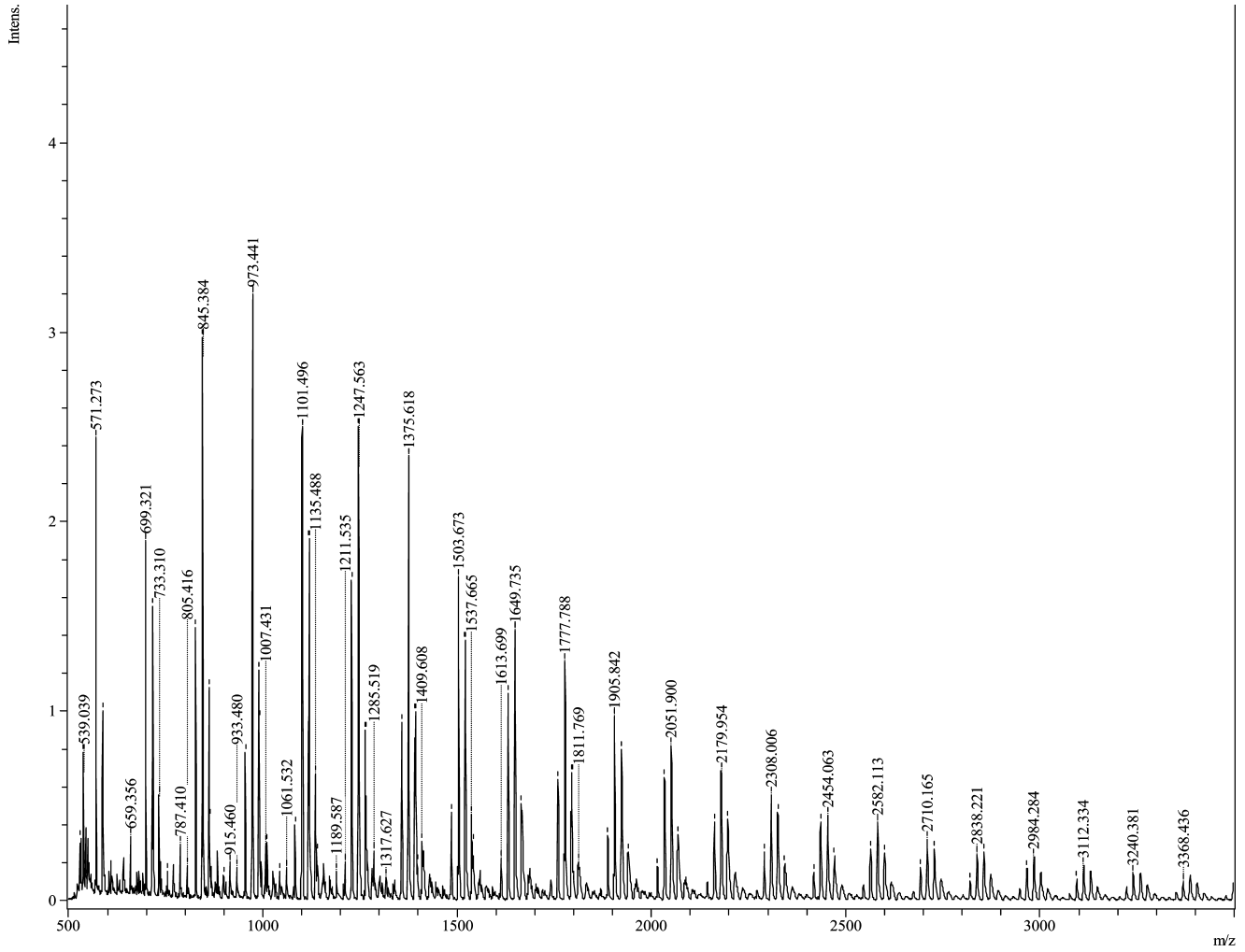

Figure 3. MALDI-TOF MS spectrum of PGaAd.

$$n = \frac{E^*}{3RT} \quad (2)$$

In eq 2, n is the cross-linking density, E^* corresponds to Young's modulus, R represents the gas constant, and T signifies the temperature. The temperature was assumed constant (37 °C = 310 K). The cross-linking values increased with an increase in modulus values (Table 1). With a higher degree of cross-linking, increase in modulus values can be observed. This trend was reported in earlier studies.[34] As discussed in the previous sections, the functional groups of GO contributed to the increase in cross-linking in the composites. The cross-linking density was the highest for 1 wt % GO composite and the lowest for PGaAd.

2.2.6. Surface Water Wettability. The contact angle measurements revealed that the composites became slightly hydrophilic with an increase in the GO content (Table 1). The presence of hydrophilic polar functional groups contributes to the hydrophilicity of GO.[3,35] The contact angles decreased from 86 to 82° with the addition of 1 wt % GO to PCL, which is similar to the composite studied here, where the contact angle decreased from 82 to 78° with the addition of 1 wt % GO to PGaAd.[3]

2.2.7. Scanning Electron Microscopy (SEM). SEM images (Figure 4) revealed that GO flakes were uniformly distributed in the case of PGaAdGO0.5 and PGaAdGO1.

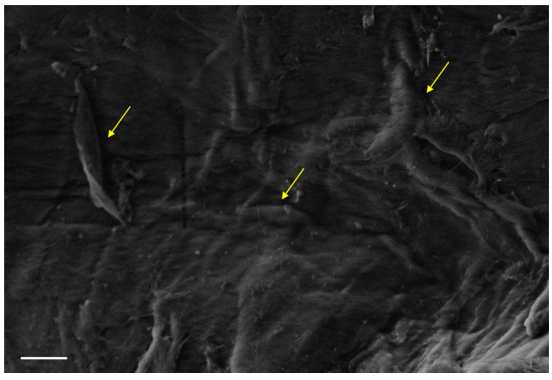

Figure 4. SEM image of GO in PGaAdGO1. The scale bar indicates 2 μm at 15 000× magnification. The yellow arrows point to GO.

2.2.8. In Vitro Hydrolytic Degradation and Kinetics. It is vital to study the degradation of the polymer to enable a good match in the time scale of the scaffold degradation and tissue regeneration at the implanted site. As the polymer degrades, the leaching of acids will reduce the pH that has a significant effect on hydrolysis. Phosphate-buffered saline (PBS) is used to maintain the pH and to reduce the effect of pH on hydrolysis. PBS is widely used for hydrolytic degradation studies.[36,37] Degradation was also conducted to study the effect of

DOI: 10.1021/acsomega.7b01139
ACS Omega 2017, 2, 5545−5556

nanofillers on the degradation of the polymer. In the case of PGaAd, 100% degradation occurred in 120 h (Figure 5).

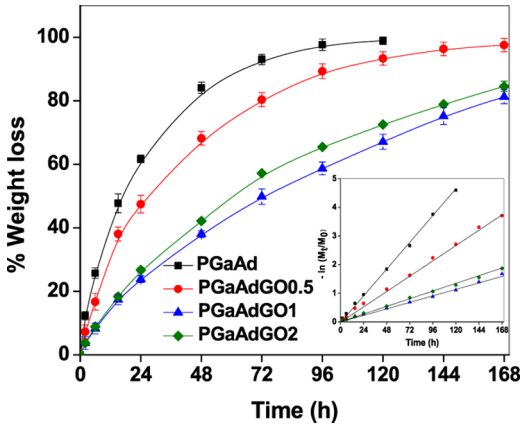

Figure 5. In vitro hydrolytic degradation profiles of PGaAd and composites in 20 mL of PBS solution (pH = 7.4). The insets show the variation of $-\ln(M_t/M_0)$ with time, and the degradation rate constants are determined from the slopes of the linear plots and are tabulated in Table 1.

However, only 93 and 68% degradations were observed in the case of PGaAdGO0.5 and PGaAdGO1. The degradation was higher in the case of PGaAdGO2, which was 73% in 120 h. For PGaAdGO0.5, PGaAdGO1, and PGaAdGO2, 98, 82, and 86% degradations were observed in a week, respectively. The trend was similar to that of modulus. This could be attributed to the increased chemical interactions between the functional groups of GO and PGaAd, as described above. Agglomeration of nanoparticles results in increased defects in the polymer, which could accelerate the degradation process. Incorporation of fillers, like clay, increased the stability of the polyesters and thereby exhibited slower degradation.[38]

Power law was used to model the rate of the degradation as follows

$$\frac{dM}{dt} = -k_d M^n \tag{3}$$

In eq 3, M is associated to the mass of the polymer, t denotes time, k_d signifies the degradation rate constant, and n represents the order of the degradation. In this case, the first-order degradation was observed for all of the polymers. The linear plots of $-\ln(M_t/M_\infty)$ with time when $n = 1$ are shown as insets in Figure 5. The intercepts were 0, and the slopes yielded k_d values, which are tabulated in Table 1.

The trend for the values of the rate coefficients, k_d, was similar to that of the degradation. PGaAd showed the highest degradation rate, which was 39.1×10^{-3} h^{-1}, whereas the lowest one was for PGaAdGO1, which was 9.7×10^{-3} h^{-1}. The degradation rate of PGaAd is approximately 4 times higher than that of PGaAdGO1. It is also approximately 3.5 and 1.7 times higher than that of PGaAdGO2 and PGaAdGO0.5, respectively. Thus, it can be concluded that the incorporation of nanoparticles slowed down the degradation process.

2.2.9. In Vitro Dye Release and Kinetics. The drug release kinetics is influenced by a number of factors, such as hydrophobicity, cross-linking, degradation, diffusion, dispersion of drugs inside the polymer, etc.[34,39] The trend of the release of the dyes was similar to that of the degradation data (Figure 6). Rhodamine B (RB) and rhodamine B base (RBB) were loaded

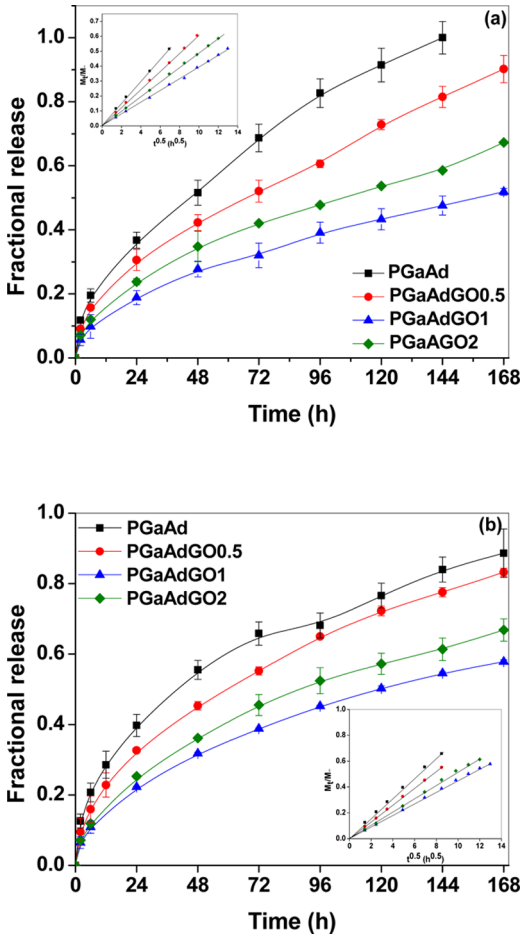

Figure 6. In vitro dye release profiles of PGaAd and composites in 20 mL of PBS solution (pH = 7.4). Release of (a) RB and (b) RBB. The insets of all of the plots show the variation of M_t/M_∞ with $t^{0.5}$, and the release rate constant, k_{RB} and k_{RBB}, are obtained from the slopes of the linear plot and are tabulated in Table 1.

into the composites and PGaAd to study the capability of release of both hydrophilic and hydrophobic drugs. In the case of RB (Figure 5a), 100% release was observed for PGaAd in 144 h. However, only 82, 59, and 48% releases were observed for PGaAdGO0.5, PGaAdGO2, and PGaAdGO1, respectively. For PGAGO0.5, PGAGO2, and PGaAdGO1, 90, 67, and 57% releases were observed in a week, respectively. In the case of RBB (Figure 5b), 89, 82, 67, and 54% releases were observed for PGaAd, PGaAdGO0.5, PGaAdGO2, and PGaAdGO1 in a week, respectively. This could be attributed to the increased stability for reduced release and possibility of agglomeration for increased release as explained in the In Vitro Hydrolytic Degradation and Kinetics section above.

As the trend of release was similar to that of degradation, it is clear that the release was mainly governed by the degradation of the polymer and composites. In addition, diffusion played a crucial role because the release of the dyes happened followed by water inflow. This could be ascribed to the slightly slower release of RBB when compared to that of RB because of its hydrophobic nature. The same trends were reported when the release of RBB was slower than that of RB.[40]

The dye release was modeled by the Korsmeyer–Peppas model,[41] which is given by

DOI: 10.1021/acsomega.7b01139
ACS Omega 2017, 2, 5545−5556

$$\frac{M_t}{M_\infty} = kt^n \quad (4)$$

In eq 4, M_t/M_∞ denotes the fraction of the quantity of the dye released at the desired time duration t and at infinite time, respectively. k signifies the rate constant, and n corresponds to the release exponent, explaining the mechanism of the dye/drug transport inside the polymer. The power law holds true only for first 60% of the drug release profile.[42] M_t/M_∞ versus time was plotted on a log−log plot (as shown in the insets of Figure 6a,b), and the data were fitted with $n = 0.5$, indicative of Higuchi kinetics/Fickian diffusion.[43] The release rate coefficients were calculated on the basis of the initial slopes with 0 intercept and are tabulated in Table 1.

The trends of dye release rate coefficients were similar to those of dye release. In the case of RB, k_{RB} of PGaAd was approximately 1.7, 1.5, and 1.2 times greater than that of PGaAdGO0.5, PGaAdGO2, and PGaAdGO1, respectively. Similarly, in the case of RBB, k_{RBB} of PGaAd was approximately 1.9, 1.6, and 1.2 times greater than that of PGaAdGO0.5, PGaAdGO2, and PGaAdGO1, respectively.

It is also worth noting that the dye release was slower than degradation. For example, in the case of RB, 100% degradation of PGaAd was observed in 120 h, whereas complete release from PGaAd occurred only in 144 h. The FTIR spectra of the physical mixtures of the dye and composites were compared with the spectra of the polymer containing dye after curing (FTIR spectra not shown). The spectra indicated that the −COOH and $-OCH_3$ groups of the dye reacted with the functional groups of the polymer, which resulted in a slower release and is consistent with earlier studies.[40]

2.2.10. Cytocompatibility Studies. 2.2.10.1. Water-Soluble Tetrazolium Salts (WST) Assay. The cytocompatibility was studied by measuring the number of live cells that result in yellow formazan in the WST assay. The obtained absorbance values are converted to the number of cells based on a previously obtained calibration curve. The assay proved that PGaAd and all of the composites were minimally cytotoxic (Figure 7). No significant differences were found in cell numbers for PGaAd and PGaAdGO0.5 with tissue culture polystyrene (TCPS). Despite the statistically significant differences between the control (TCPS) and the samples on day 3, the cell numbers doubled from day 1 to day 3 in all cases, implying that the cells proliferated well and these samples were cytocompatible. PGaAd showed the least increase in cell numbers. This could be attributed to the leaching of acids, which will result in the change of pH to acidic. An acidic environment is not friendly for the survival for cells. When these materials are placed inside the body, the toxicity is minimized because there will be a large amount of continuous blood flow in our body and the acids if leached will be minimal and washed out. However, the hydrolysis rate of a degradable material can cause inflammation in animal tissue and would need further investigation.

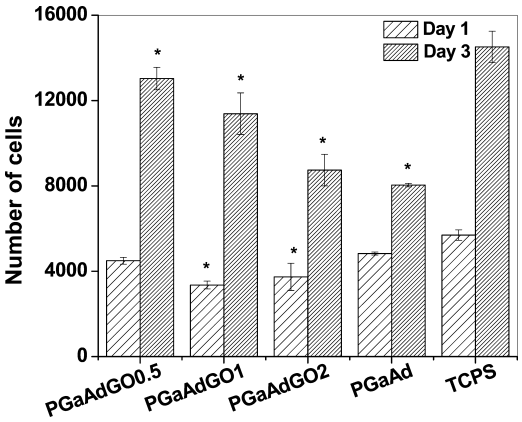

Figure 7. Cell viability of PGaAd and composites determined by the WST assay for day 1 and day 3. *The samples are statistically significant when compared to the control.

The cell numbers were higher in the case of composites, whereas the highest cell numbers were found in the case of control. Among the composites, PGaAdGO0.5 showed the highest cell numbers, from 4500 to 13 000. This was followed by PGaAdGO1, which showed an increase in cell numbers from 3350 to 11 400. PGaAdGO2 showed an increase in cell numbers from 3740 to 8740. This can be attributed to the presence of hydrophilic functional groups present in GO that contributed to the increase in cell attachment. The hydrophilicity was further verified by contact angle measurements. The increase in cell number decreased with an increase in the GO content. Incorporation of nanoparticles resulted in the reduction in toxicity of the polymer as well as improved the biological response of the biomaterial.[44] However, with an increase in the concentration of GO, it could induce slight toxicity, as observed in our study. It was demonstrated that GO in higher concentration can induce oxidative stress based on dose and size.[45]

2.2.10.2. Live/Dead Assay. Live/dead assay was used to measure fractional cell viability. Live cells were stained green, and dead cells were stained red.[46] The images supported the data of the WST assay (Figure 8). The number of viable cells was the highest in the case of control. The viable cells were the least in PGaAd. All of the composites exhibited a higher number of viable cells when compared to those in PGaAd and lesser number of viable cells when compared to those in the control. As described in the previous section, the higher number of viable cells was observed in PGaAdGO0.5, whereas the least number of viable cells was observed in PGaAdGO2.

2.2.10.3. DNA Quantification Assay. The DNA content increased from day 14 to day 21 on PGaAd and PGaAdGO1 films and control (Figure 9). The differences between the DNA content in the samples and TCPS were statistically significant on both day 14 and day 21. This could be associated with the hydrophobic nature of PGaAd where the initial cell attachment could be low, and it was significantly better in the case of slightly hydrophilic PGaAdGO1. Nevertheless, the increase in DNA content on both the samples indicated that these composites may induce better cell adhesion and proliferation. The values of DNA content in the case of PGaAd increased to 3370 ng on day 21 from 2300 ng on day 14. In the case of PGaAdGO1, the DNA content increased from 3900 ng on day 14 to 4800 ng on day 21. In the case of TCPS, the DNA content increased from 5000 ng on day 14 to 6000 ng on day 21. The presence of hydrophilic functional groups in GO facilitated better cell attachment and proliferation in the case of PGaAdGO1 when compared to that in PGaAd. Hydrophilic surfaces demonstrate better cell adhesion and growth as they mediate the binding of cell adhesive proteins, such as fibronectin and vitronectin.[47] Although the cell attachment and proliferation were lesser on samples, they induced osteogenesis better than that by the control, as explained later.

DOI: 10.1021/acsomega.7b01139
ACS Omega 2017, 2, 5545−5556

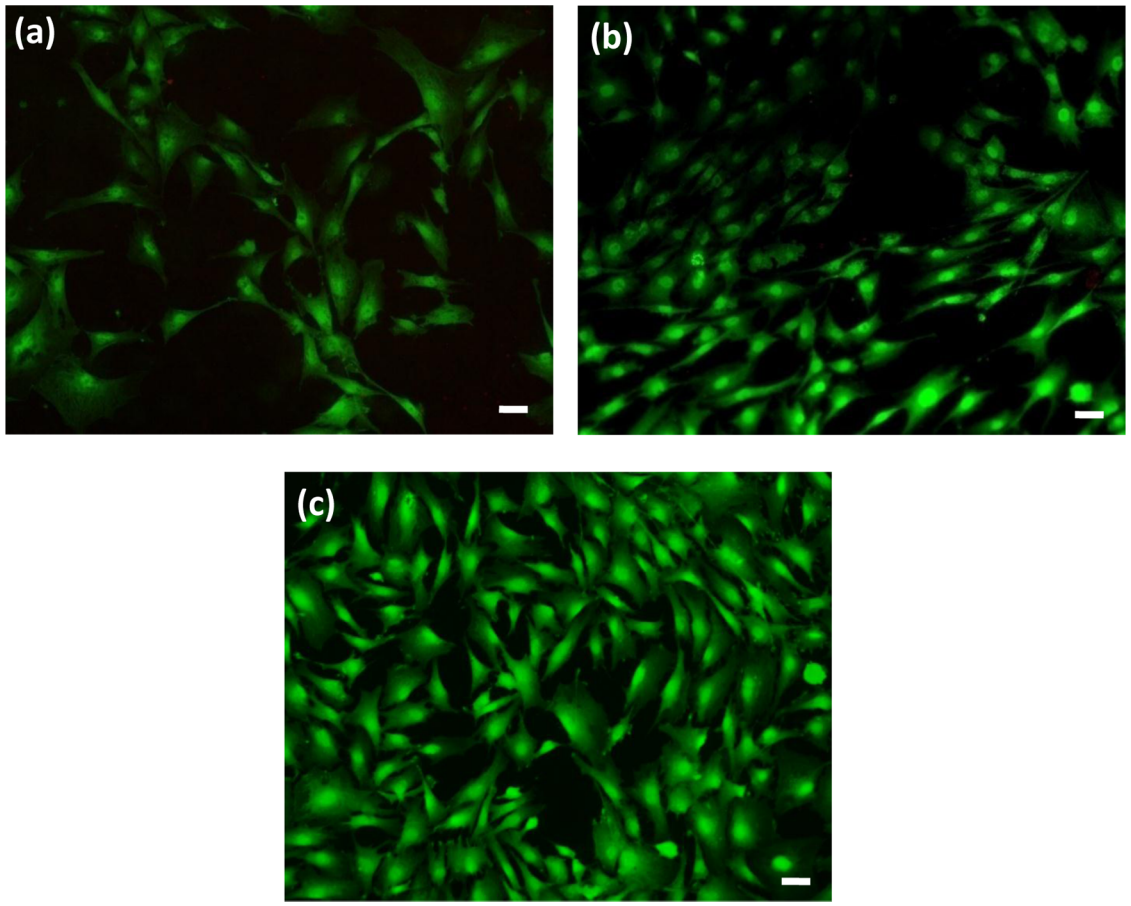

Figure 8. Fluorescent images of the viability assay performed for various polyesters on day 3: (a) PGaAd, (b) PGaAdGO1, and (c) TCPS. The scale bar indicates 20 μm. All images are taken at 4× magnification. Viable cells appear green, whereas nonviable cells appear red.

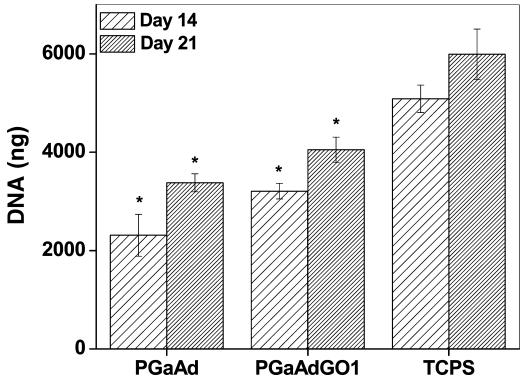

Figure 9. DNA quantification of MC3T3 cells cultured on polymer films of PGaAd and PGaAdGO1 by the PicoGreen assay on day 14 and day 21. *The samples are statistically significant ($p < 0.05$) when compared to the control. The results represent average ± standard deviation (SD) for $n = 3$.

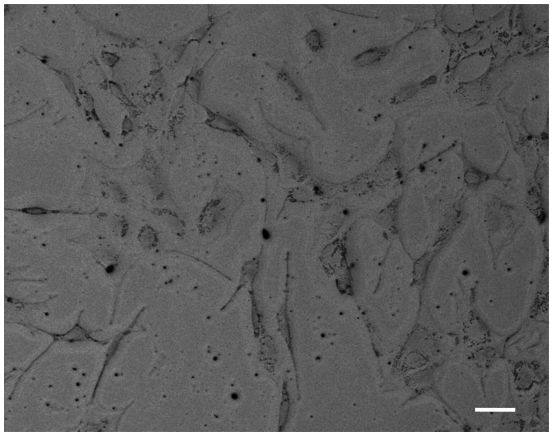

Figure 10. Optical micrographs of MC3T3 cells treated with a medium containing the degradation products of PGaAdGO1 at 10× magnification. The scale bar is 20 μm.

2.2.10.4. Cell Morphology. Examination of the morphology of the cell becomes crucial as it can be correlated to the cell function.[48] Optical bright field images (Figure 10) displayed the "spindle shaped" morphology of the cells in both the samples and the control. Good cell−cell communication was observed with well-spread appearance in both the samples and the control. This further confirmed that these polymers are cytocompatible and can be used for tissue regeneration.

2.2.11. Osteogenic Differentiation Study. 2.2.11.1. Mineralization by Alizarin Red Staining. Mineralization by alizarin red staining confirmed the presence of calcium on the films of PGaAd, PGaAdGO1, and control (Figure 11). The presence of calcium deposits by the cells can be correlated to the differentiation of preosteoblast cells into mature osteoblasts.[49] Alizarin red staining showed that there was an increase in calcium deposits from day 14 to day 21 on the films of PGaAd, PGaAdGO1, and control. The samples exhibited better calcium

DOI: 10.1021/acsomega.7b01139
ACS Omega 2017, 2, 5545−5556

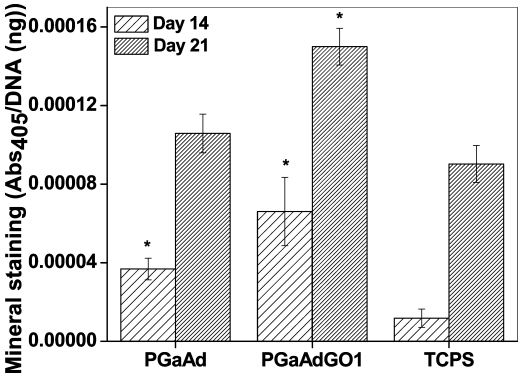

Figure 11. Quantification of cell-mediated mineral deposition by alizarin red S dye on films of PGaAd and composites on day 14 and day 21. *The samples are statistically significant ($p < 0.05$) when compared to control. The results represent average ± SD for $n = 3$.

deposition than that by control. There were statistically significant differences between calcium deposition in the films and in the control on day 14. However, on day 21, there were no statistical differences between PGaAd and control, whereas there were differences between PGaAdGO1 and control. This could be due to the relatively high modulus as it is proven that materials with a higher modulus drive osteogenesis.[50] Also, the presence of carboxyl groups in GO facilitates the binding of calcium and phosphate ions.[51,52] In addition to this, it has been reported earlier that β-glycerol phosphate in the osteoinductive medium used in this study will be absorbed by GO in the polymer and enhance osteogenesis.[5] Therefore, it can be concluded that these composites effectively induce osteogenesis.

2.2.11.2. Alkaline Phosphatase Expression. To further verify osteogenesis, alkaline phosphatase (ALP) activity expression was evaluated (Figure 12). ALP expression is an

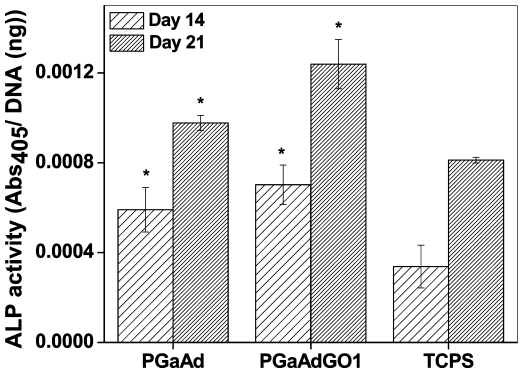

Figure 12. Quantification of ALP expression in cells on PGaAd and composites on day 14 and day 21. *The samples are statistically significant ($p < 0.05$) when compared to control. The results represent average ± SD for $n = 3$.

early marker of osteogenic differentiation.[53−55] Figure 10 compiled that the ALP activity increased from day 14 to day 21 on all films and control. The films showed higher ALP expression than control on both day 14 and day 21, and the differences were statistically significant. ALP expression increased from 1.6×10^{-4} to 3.9×10^{-4}, 7×10^{-4} to 14.6×10^{-4}, and 3.4×10^{-4} to 8.1×10^{-4} in the case of PGaAd, PGaAdGO1, and control, respectively, from day 14 to day 21. As explained in the earlier section, the presence of −COOH and −OH groups in GO enhances osteogenesis and upregulates osteogenic gene expression.[56] The incorporation of GO can serve as an alternate for the modification of biomaterials by incorporating biomolecules such as bone morphogenic protein[57] to enhance osteogenesis. The incorporation of GO has several advantages, such as stability, low cost, and easy processing.[53] The above studies illustrated that these polymers direct cells toward osteogenic lineage. These polymers can be further tested in vivo to evaluate the osteogenic abilities.

3. CONCLUSIONS

Nanocomposites with different weight percentages of GO in galactitol-based polyesters were prepared. Glass-transition temperature and modulus increased, whereas contact angle decreased with an increase in weight percentages of GO. The degradation and dye release studies showed that the degradation and release decreased with an increase in weight percentages of GO, whereas for 2 wt % GO, the degradation and release increased. The degradation followed first-order kinetics, whereas the dye release followed Higuchi kinetics. PGaAdGO1 exhibited a higher modulus and slower degradation. Cytocompatibility studies showed that these composites are minimally cytotoxic. Osteogenic differentiation studies proved that PGaAdGO1 exhibited significant efficiency in dictating the cells toward osteogenesis.

4. MATERIALS AND METHODS

4.1. Materials. Graphite flakes were purchased from Supreme Company, India. Sulfuric acid, phosphoric acid, hydrochloric acid, potassium permanganate, hydrogen peroxide, and solvent DMF were procured from Merck, India. Galactitol, a polyol, was purchased from TCI Chemicals, Japan. Adipic acid was purchased from Sigma-Aldrich.

4.2. Synthesis of PGA. The synthesis method was similar to that in the previous report.[20] Galactitol and adipic acid were taken in the molar ratio of 1:1 in a 50 mL round-bottomed flask. The melt condensation reaction was performed under the experimental conditions of 180 °C for 2 h in the presence of nitrogen atmosphere. The prepolymer obtained (85−90% yield) was further thermally cured at 120 °C under vacuum for 3 days (Scheme 1).

4.3. Preparation of GO. The preparation of GO was done by the chemical oxidation of graphite flakes based on the Hummers method.[58] Graphite flakes (1 g) were added to the round-bottomed flask containing a mixture of 55 mL of sulfuric acid and 7 mL of phosphoric acid. The mixture was stirred under ice bath for 30 min for exfoliation of flakes. Potassium permanganate (6 g) was added to the mixture for oxidation and was stirred for 3 days at 25 °C. Followed by this, hydrogen peroxide was added to halt the reaction and to remove the excess potassium permanganate. The GO obtained was washed with 1 M hydrochloric acid and deionized (DI) water for 2 weeks. Later, GO was obtained by centrifugation at 10 000 rpm for 1 h and dried at 25 °C for 3 days. This was followed by vacuum oven drying at 40 °C for 1 week.

4.4. Preparation of GO/Polymer Nanocomposite. The prepolymer of PGaAd was dissolved in DMF. Separately, GO was dispersed in DI water. The weight percentages of GO were 0.5, 1, and 2% of the total weights of PGA taken. The GO/polymer nanocomposites were prepared individually by mixing the appropriate weight percentage of GO dispersed in water

DOI: 10.1021/acsomega.7b01139
ACS Omega 2017, 2, 5545−5556

and PGaAd solution. DMF and water were miscible, and no phase separation was observed. DMF and water were evaporated in a thermal oven. Later, the polymer along with GO was thermally cured, as described in Section 4.2, resulting in the formation of the nanocomposites.

4.5. Characterization and Studies of Nanocomposites. Proton nuclear magnetic resonance (^{1}H NMR) and matrix-assisted laser desorption ionization time-of-flight mass spectrometry (MALDI-TOF MS) were performed for the prepolymer as the cured polymers are insoluble in solvents.

4.5.1. FTIR Spectroscopy. FTIR was performed on PGaAd and nanocomposites before and after curing using attenuated total reflectance (U-ATR, PerkinElmer FTIR Spectrum BX) mode. Scanning was performed in the range of 600−4000 cm^{-1} with the average of 12 scans and 4 cm^{-1} resolution on all samples.

4.5.2. ^{1}H NMR Spectroscopy. Proton nuclear magnetic resonance (^{1}H NMR) was performed for PGaAd using a 400 MHz Bruker NMR spectrometer. The prepolymer was dissolved in deuterated DMSO, which had internal calibration.

4.5.3. Differential Scanning Calorimetry. Differential scanning calorimetry (DSC; TA Instruments) was performed to determine the thermal properties of PGaAd and nanocomposites. Samples weighing 3−5 mg were taken in aluminum pans and heated and cooled in the range of −50 to 200 °C at the rate of 10 °C/min in the presence of nitrogen atmosphere. To eliminate the processing information, the heating and cooling cycle was repeated again.

4.5.4. Matrix-Assisted Laser Desorption Ionization Time-of-Flight Mass Spectrometry (MALDI-TOF MS). MALDI-TOF MS was performed to find the molecular weight of the prepolymer (UltrafleXtreme MALDI Bruker Daltonics) of PGaAd. The prepolymer was dissolved in DMF/acetonitrile mixture before analysis.

4.5.5. Dynamic Mechanical Analysis. The mechanical properties of PGaAd and nanocomposites were investigated by DMA (Q800; TA Instruments). Films of PGaAd and nanocomposites were cut in accordance with the dimensions (30 mm × 5 mm × 1 mm). Frequency sweep from 1 to 10 Hz at 37 °C, 15 μm amplitude, and preload of 0.01 N were used as operational conditions. A tension clamp designed for film/fiber was used.

4.5.6. Surface Water Wettability. The water contact angles of PGaAd and nanocomposites were measured using a goniometer (Data Physics). DI water droplet (1 μL) was placed on the surface of the films, and sufficient time was provided for the attainment of equilibrium. The readings were taken, and the data are presented as mean ± standard deviation of three independent readings.

4.5.7. Scanning Electron Microscopy. Scanning electron microscopy (SEM; Zeiss) was performed to observe the distribution of GO sheets in the polymer. Gold coating was performed for 100 s to achieve a 10 nm coating.

4.5.8. In Vitro Hydrolytic Polymer Degradation. PGaAd and nanocomposites were punched as round disks of dimensions 4.5 mm × 1 mm at 25 °C. These samples were transferred to nylon mesh bags and submerged in 50 mL centrifuge tubes containing 20 mL of PBS of pH 7.4. These disks were moved to an incubator shaker maintained at 37 °C and shaking at 100 rpm. The samples were rinsed in water and dried in a hot air oven to obtain a constant weight at fixed time points. PBS was refreshed every day to avoid the effects caused due to pH variations.

The differences in the mass of the samples after drying at every time point were used to calculate their mass loss. It was calculated using eq 5

$$\%\ \text{mass loss} = (M_o - M_t)/M_o \times 100 \quad (5)$$

where M_o is the initial mass of the polymer and M_t is the mass of the samples after degradation at the desired time interval.

4.5.9. In Vitro Dye Release. PGaAd and nanocomposites before curing were mixed with dyes of both hydrophilic and hydrophobic nature to assess their release capabilities. Two dyes belonging to a similar family, RB and RBB, were chosen. DMF was used as a common solvent to dissolve polymer/GO and the dyes (5 wt %). The solvent was evaporated, leaving behind a homogeneous mixture of polymer/GO along with dyes. This mixture was cured, and disks were punched out for the studies. They were placed in 20 mL of PBS of pH 7.4 and moved to the incubator shaker with an agitation of 100 rpm and 37 °C. PBS was replenished every day. PBS (100 μL) containing dye was collected at desired time durations in a 96-well plate for each sample. The quantity of the dye released was assessed using a microplate reader (BioTek Synergy HT) with the wavelength adjusted to 553 nm. Using the calibration curves, the concentrations of the dyes were obtained from the absorbance values. The polymers were dissolved in a basic solution of NaOH, and the total concentration of the loaded dye was calculated. On the basis of the total concentration, the fractional concentration of the dye released at each time point and cumulative release were calculated.

4.5.10. Cytocompatibility of the Polymer. 4.5.10.1. Cell Culture. As these composites were intended for use in bone tissue engineering applications, it is necessary to study the cytocompatibility property using osteoblasts. MC3T3-E1 cells (subclone 4), which are mouse calvarial preosteoblasts (American Type Culture Collection), were used. The α-minimum essential medium (Sigma) with 1% antibiotics (Sigma) and fetal bovine serum (10% v/v; Gibco, Life Technologies) was used to culture the cells in T-75 flasks (maintained at 37 °C, 5% CO_2).

4.5.10.2. Cell Viability. The sterilized (UV-treated) polymer disks were placed in 5 mL of cell culture medium (one disc in each centrifuge tube), and they were maintained for 24 h in a CO_2 incubator (37 °C). Thus, a conditioned medium was obtained (the medium with the degradation products of the polymer). Triplicates were used for PGaAd and each composite type. Simultaneously, 2000 cells in 200 μL of culture medium were added to each well in a 96-well plate. They were left for 12 h for effective cell attachment and cell proliferation before replacing them with conditioned media. Fresh medium was added to the cells that served as controls. Cell viability and cell morphology were examined after the cells were exposed to the conditioned media for 1 day and 3 days.

Cell viability was studied using the WST-1 assay. A single well was assigned for each of the triplicates of PGaAd and composite type for two time points ($n = 4 \times 3 \times 2 = 24$). Three wells were used as controls without polymers at all time points ($n = 3 \times 2 = 6$). The WST reagent (Roche) was prepared in the working concentration of 10/100 μL media per well and added to each well. The well plate was kept in a CO_2 incubator for 1 h till the color change of the media to yellow. Using a microplate reader, the absorbance was measured at 440 nm.

4.5.10.3. Live/Dead Assay. Cell viability was also verified qualitatively by the live/dead fluorescence cytotoxicity assay (Molecular Probes, Invitrogen). Live and dead cells were

DOI: 10.1021/acsomega.7b01139
ACS Omega 2017, 2, 5545−5556

stained using 2 mM calcein dye and 4 mM ethidium homodimer, respectively. These dyes were allowed to bind for 15 min in a CO_2 incubator at 37 °C and removed later to avoid false positive results. They were imaged using a fluorescent microscope (Olympus).

4.5.10.4. Cell Proliferation. Cell proliferation was evaluated using the PicoGreen assay that is based on DNA quantification[1] on the surface of PGaAd and PGaAdGO1 films based on the highest moduli and slow degradation. Cells (4×10^3) were seeded onto the surface of the films (2D films of PGaAd and PGaAdGO1). At 14 days and 21 days time points, 0.2 mL of lysis solution with 0.2 mg/mL proteinase K and 0.02% sodium dodecyl sulfate (SDS) was added after the medium removal. The incubation time was 12 h at 25 °C. This mixture (0.1 mL) was taken and PicoGreen dye (0.1 mL; 5 μg/mL in 1× Tris−ethylenediaminetetraacetic acid buffer) was added to this mixture. The fluorescence intensity was measured at 480 nm excitation and 520 nm emission using a microplate reader. The DNA was quantified using a standard curve based on serial dilutions of known DNA concentration. Cells cultured on TCPS were used as controls.

4.5.10.5. Cell Morphology. For studying cell morphology, the cells were fixed by 3.7% formaldehyde (Merck) for 15 min. The cells were given water wash before bright field imaging (Olympus).

4.5.11. Osteogenic Differentiation Study. Osteogenic differentiation was illustrated by the mineralization deposits and measuring alkaline phosphatase activity based on culturing MC3T3 cells onto the surface of PGaAd and PGaAdGO1 films. This composite was selected on the basis of the highest storage modulus and slow degradation among the polymers studied. Complete knockout Dulbecco's modified Eagle's medium supplemented with β-glycerol phosphate (10 mM) and ascorbic acid (25 μM) (Sigma) was used to culture the cells that are capable of osteogenesis as reported.[59]

4.5.11.1. Alizarin Red Staining. Calcium mineralization was studied at day 14 and day 21. At these time points, the cells were fixed (3.7% formaldehyde for 15 min, as described earlier). Alizarin red stain (Sigma) was used to quantify calcium deposits. The filtered dye was added to the cells. Quadruplicates were used for PGaAd and PGaAdGO1. TCPS served as the control. The dye binds to the calcium present in the films. Later, the samples were washed with water until a clear solution was obtained after the removal of dye that was not bound to calcium to avoid increased absorbance values. The dye that was bound to calcium in the films was dissolved using 5% SDS in 0.5 HCl for 25 min. Using a microplate reader, the absorbance values were measured at 405 nm. The values were normalized to those of the cell numbers obtained from the PicoGreen assay.

4.5.11.2. Alkaline Phosphatase Activity. The ALP was quantified on day 14 and day 21 by the *p*-nitrophenyl phosphate dye (Sigma).[54] Lysis solution, 200 μL, comprising 0.2% Triton X-100 was used to lyse the cells for 12 h. Later, the mixture was freeze−thawed from −80 to 37 °C at least three times. To the lysis solution, equal amount of dye was added in 96-well plates, and the absorbance values were measured using a microplate reader at 405 nm. The values were normalized to the cell numbers obtained from the PicoGreen assay.

4.5.12. Statistical Analysis. One-way analysis of variance with Tukey's test was performed to assess the significant differences across the samples and controls. *p* Values less than 0.05 were considered to be statistically significant.

AUTHOR INFORMATION

Corresponding Author

*E-mail: kchatterjee@materials.iisc.ernet.in. Tel: 91-80-22933408. Fax: 91-80-23600472.

ORCID

Giridhar Madras: 0000-0003-2211-5055

Kaushik Chatterjee: 0000-0002-7204-2926

Notes

The authors declare no competing financial interest.

ACKNOWLEDGMENTS

This work was funded by the Department of Biotechnology (DBT), India (BT/PR5977/MED/32/242/2012). G.M. is grateful for J.C. Bose fellowship from DST, India. We acknowledge Queeny Dasgupta for help with DSC thermograms and DMA analysis. We are grateful to Sai Rama Krishna Meka for technical assistance with cell studies. We thank Sumit Bahl and N.K.R. Eswar for assistance with the contact angle measurements and SEM analysis. We thank NMR Research Centre for access to NMR.

REFERENCES

(1) Kumar, S.; Chatterjee, K. Strontium eluting graphene hybrid nanoparticles augment osteogenesis in a 3D tissue scaffold. *Nanoscale* **2015**, *7*, 2023−2033.

(2) Lips, P. A. M.; van Luyn, M. J. A.; Chiellini, F.; Brouwer, L. A.; Velthoen, I. W.; Dijkstra, P. J.; Feijen, J. Biocompatibility and degradation of aliphatic segmented poly(ester amide)s: in vitro and in vivo evaluation. *J. Biomed. Mater. Res., Part A* **2006**, *76A*, 699−710.

(3) Kumar, S.; Raj, S.; Kolanthai, E.; Sood, A. K.; Sampath, S.; Chatterjee, K. Chemical functionalization of graphene to augment stem cell osteogenesis and inhibit biofilm formation on polymer composites for orthopedic applications. *ACS Appl. Mater. Interfaces* **2015**, *7*, 3237−3252.

(4) Zhang, Y.; Nayak, T. R.; Hong, H.; Cai, W. Graphene: a versatile nanoplatform for biomedical applications. *Nanoscale* **2012**, *4*, 3833−3842.

(5) Lee, W. C.; Lim, C. H. Y. X.; Shi, H.; Tang, L. A. L.; Wang, Y.; Lim, C. T.; Loh, K. P. Origin of enhanced stem cell growth and differentiation on graphene and graphene oxide. *ACS Nano* **2011**, *5*, 7334−7341.

(6) Ramanathan, T.; Abdala, A. A.; Stankovich, S.; Dikin, D. A.; Herrera-Alonso, M.; Piner, R. D.; Adamson, D. H.; Schniepp, H. C.; Chen, X.; Ruoff, R. S.; et al. Functionalized graphene sheets for polymer nanocomposites. *Nat. Nanotechnol.* **2008**, *3*, 327−331.

(7) Chen, G.-Y.; Pang, D. W.-P.; Hwang, S.-M.; Tuan, H.-Y.; Hu, Y.-C. A graphene-based platform for induced pluripotent stem cells culture and differentiation. *Biomaterials* **2012**, *33*, 418−427.

(8) Liu, C.-W.; Xiong, F.; Jia, H.-Z.; Wang, X.-L.; Cheng, H.; Sun, Y.-H.; Zhang, X.-Z.; Zhuo, R.-X.; Feng, J. Graphene-based anticancer nanosystem and its biosafety evaluation using a zebrafish model. *Biomacromolecules* **2013**, *14*, 358−366.

(9) Carpio, I. E. M.; Santos, C. M.; Wei, X.; Rodrigues, D. F. Toxicity of a polymer−graphene oxide composite against bacterial planktonic cells, biofilms, and mammalian cells. *Nanoscale* **2012**, *4*, 4746−4756.

(10) Bao, H.; Pan, Y.; Ping, Y.; Sahoo, N. G.; Wu, T.; Li, L.; Li, J.; Gan, L. H. Chitosan-functionalized graphene oxide as a nanocarrier for drug and gene delivery. *Small* **2011**, *7*, 1569−1578.

(11) Kim, T.-H.; Shah, S.; Yang, L.; Yin, P. T.; Hossain, M. K.; Conley, B.; Choi, J.-W.; Lee, K.-B. Controlling differentiation of adipose-derived stem cells using combinatorial graphene hybrid-pattern arrays. *ACS Nano* **2015**, *9*, 3780−3790.

(12) Vilela, C.; Sousa, A. F.; Fonseca, A. C.; Serra, A. C.; Coelho, J. F. J.; Freire, C. S. R.; Silvestre, A. J. D. The quest for sustainable polyesters—insights into the future. *Polym. Chem.* **2014**, *5*, 3119−3141.

DOI: 10.1021/acsomega.7b01139
ACS Omega 2017, 2, 5545−5556

(13) Wang, Y.; Kim, Y. M.; Langer, R. In vivo degradation characteristics of poly(glycerol sebacate). *J. Biomed. Mater. Res., Part A* **2003**, *66A*, 192−197.
(14) Ensminger, M. E., Ensminger, A. H., Eds. *Foods & Nutrition Encyclopedia*, 2nd ed.; CRC Press: Boca Raton, 1993; pp 1−1216.
(15) Natarajan, J.; Dasgupta, Q.; Shetty, S. N.; Sarkar, K.; Madras, G.; Chatterjee, K. Poly(ester amide)s from Soybean Oil for Modulated Release and Bone Regeneration. *ACS Appl. Mater. Interfaces* **2016**, *8*, 25170−25184.
(16) Depan, D.; Girase, B.; Shah, J. S.; Misra, R. D. K. Structure−process−property relationship of the polar graphene oxide-mediated cellular response and stimulated growth of osteoblasts on hybrid chitosan network structure nanocomposite scaffolds. *Acta Biomater.* **2011**, *7*, 3432−3445.
(17) Girase, B.; Shah, J. S.; Misra, R. D. K. Cellular mechanics of modulated osteoblasts functions in graphene oxide reinforced elastomers. *Adv. Eng. Mater.* **2012**, *14*, B101−B111.
(18) Wang, K.; Ruan, J.; Song, H.; et al. Biocompatibility of graphene oxide. *Nanoscale Res. Lett.* **2011**, *6*, 8.
(19) Mu, Q.; Su, G.; Li, L.; Gilbertson, B. O.; Yu, L. H.; Zhang, Q.; Sun, Y.-P.; Yan, B. Size-dependent cell uptake of protein-coated graphene oxide nanosheets. *ACS Appl. Mater. Interfaces* **2012**, *4*, 2259−2266.
(20) Natarajan, J.; Madras, G.; Chatterjee, K. Localized delivery and enhanced osteogenic differentiation with biodegradable galactitol polyester elastomers. *RSC Adv.* **2016**, *6*, 61492−61504.
(21) Zhang, Y.; Ali, S. F.; Dervishi, E.; Xu, Y.; Li, Z.; Casciano, D.; Biris, A. S. Cytotoxicity effects of graphene and single-wall carbon nanotubes in neural phaeochromocytoma-derived PC12 cells. *ACS Nano* **2010**, *4*, 3181−3186.
(22) Coates, J. Interpretation of Infrared Spectra, a Practical Approach. In *Encyclopedia of Analytical Chemistry*; Meyers, R. A., Ed.; Wiley: Chichester, 2000; pp 10815−10837.
(23) Ren, P.-G.; Yan, D.-X.; Ji, X.; Chen, T.; Li, Z.-M. Temperature dependence of graphene oxide reduced by hydrazine hydrate. *Nanotechnology* **2010**, *22*, No. 055705.
(24) Jacobsen, N. E. *NMR Spectroscopy Explained: Simplified Theory, Applications and Examples for Organic Chemistry and Structural Biology*; John Wiley & Sons: New Jersey, 2007; p 640.
(25) Liao, K.-H.; Aoyama, S.; Abdala, A. A.; Macosko, C. Does Graphene Change T_g of Nanocomposites? *Macromolecules* **2014**, *47*, 8311−8319.
(26) Potts, J. R.; Dreyer, D. R.; Bielawski, C. W.; Ruoff, R. S. Graphene-based polymer nanocomposites. *Polymer* **2011**, *52*, 5−25.
(27) Layek, R. K.; Kuila, A.; Chatterjee, D. P.; Nandi, A. K. Amphiphilic poly(N-vinyl pyrrolidone) grafted graphene by reversible addition and fragmentation polymerization and the reinforcement of poly(vinyl acetate) films. *J. Mater. Chem. A* **2013**, *1*, 10863−10874.
(28) Natarajan, J.; Madras, G.; Chatterjee, K. Tailoring the degradation rate and release kinetics from poly(galactitol sebacate) by blending with chitosan, alginate or ethyl cellulose. *Int. J. Biol. Macromol.* **2016**, *93*, 1591−1602.
(29) Gong, L.; Kinloch, I. A.; Young, R. J.; Riaz, I.; Jalil, R.; Novoselov, K. S. Interfacial stress transfer in a graphene monolayer nanocomposite. *Adv. Mater.* **2010**, *22*, 2694−2697.
(30) Kim, H.; Abdala, A. A.; Macosko, C. W. Graphene/polymer nanocomposites. *Macromolecules* **2010**, *43*, 6515−6530.
(31) Gojny, F. H.; Wichmann, M. H. G.; Fiedler, B.; Schulte, K. Influence of different carbon nanotubes on the mechanical properties of epoxy matrix composites—a comparative study. *Compos. Sci. Technol.* **2005**, *65*, 2300−2313.
(32) He, Y.; Zhang, N.; Gong, Q.; Qiu, H.; Wang, W.; Liu, Y.; Gao, J. Alginate/graphene oxide fibers with enhanced mechanical strength prepared by wet spinning. *Carbohydr. Polym.* **2012**, *88*, 1100−1108.
(33) Wan, C.; Chen, B. Poly(ε-caprolactone)/graphene oxide biocomposites: mechanical properties and bioactivity. *Biomed. Mater.* **2011**, *6*, No. 055010.
(34) Natarajan, J.; Movva, S.; Madras, G.; Chatterjee, K. Biodegradable galactitol based crosslinked polyesters for controlled release and bone tissue engineering. *Mater. Sci. Eng., C* **2017**, *77*, 534−547.
(35) Wang, S.; Zhang, Y.; Abidi, N.; Cabrales, L. Wettability and surface free energy of graphene films. *Langmuir* **2009**, *25*, 11078−11081.
(36) Bruggeman, J. P.; de Bruin, B.-J.; Bettinger, C. J.; Langer, R. Biodegradable poly(polyol sebacate) polymers. *Biomaterials* **2008**, *29*, 4726−4735.
(37) Grizzi, I.; Garreau, H.; Li, S.; Vert, M. Hydrolytic degradation of devices based on poly(DL-lactic acid) size-dependence. *Biomaterials* **1995**, *16*, 305−311.
(38) Kumar, A. P.; Depan, D.; Tomer, N. S.; Singh, R. P. Nanoscale particles for polymer degradation and stabilization—trends and future perspectives. *Prog. Polym. Sci.* **2009**, *34*, 479−515.
(39) Natarajan, J.; Rattan, S.; Singh, U.; Madras, G.; Chatterjee, K. Polyanhydrides of castor oil−sebacic acid for controlled release applications. *Ind. Eng. Chem. Res.* **2014**, *53*, 7891−7901.
(40) Natarajan, J.; Madras, G.; Chatterjee, K. Maltitol-based biodegradable polyesters with tailored degradation and controlled release for bone regeneration. *RSC Adv.* **2016**, *6*, 40539−40551.
(41) Korsmeyer, R. W.; Gurny, R.; Doelker, E.; Buri, P.; Peppas, N. A. Mechanisms of solute release from porous hydrophilic polymers. *Int. J. Pharm.* **1983**, *15*, 25−35.
(42) Costa, P.; Lobo, J. M. S. Modeling and comparison of dissolution profiles. *Eur. J. Pharm. Sci.* **2001**, *13*, 123−133.
(43) Natarajan, J.; Chatterjee, K.; Madras, G. Tailored Degradation and Dye Release from Poly(ester amides). *Polym.—Plast. Technol. Eng.* **2017**, *56*, 635−646.
(44) Webb, K.; Hlady, V.; Tresco, P. A. Relative importance of surface wettability and charged functional groups on NIH 3T3 fibroblast attachment, spreading, and cytoskeletal organization. *J. Biomed. Mater. Res.* **1998**, *41*, 422.
(45) Chang, Y.; Yang, S.-T.; Liu, J.-H.; Dong, E.; Wang, Y.; Cao, A.; Liu, Y.; Wang, H. In vitro toxicity evaluation of graphene oxide on A549 cells. *Toxicol. Lett.* **2011**, *200*, 201−210.
(46) Kaneshiro, E. S.; Wyder, M. A.; Wu, Y.-P.; Cushion, M. T. Reliability of calcein acetoxy methyl ester and ethidium homodimer or propidium iodide for viability assessment of microbes. *J. Microbiol. Methods* **1993**, *17*, 1−16.
(47) Ko, Y.-M.; Lee, K.; Kim, B.-H. Effect of functional groups on biodegradation and pre-osteoblastic cell response on the plasma-polymerized magnesium surface. *Jpn. J. Appl. Phys.* **2013**, *52*, No. 01AE01.
(48) Shah, J. V. Cells in tight spaces: the role of cell shape in cell function. *J. Cell Biol.* **2010**, *191*, 233−236.
(49) Gregory, C. A.; Gunn, W. G.; Peister, A.; Prockop, D. J. An Alizarin red-based assay of mineralization by adherent cells in culture: comparison with cetylpyridinium chloride extraction. *Anal. Biochem.* **2004**, *329*, 77−84.
(50) Engler, A. J.; Sen, S.; Sweeney, H. L.; Discher, D. E. Matrix elasticity directs stem cell lineage specification. *Cell* **2006**, *126*, 677−689.
(51) Li, J.; Chen, Y.; Yin, Y.; Yao, F.; Yao, K. Modulation of nano-hydroxyapatite size via formation on chitosan−gelatin network film in situ. *Biomaterials* **2007**, *28*, 781−790.
(52) Landis, W. J.; Jacquet, R. Association of calcium and phosphate ions with collagen in the mineralization of vertebrate tissues. *Calcif. Tissue Int.* **2013**, *93*, 329−337.
(53) Kumar, S.; Raj, S.; Sarkar, K.; Chatterjee, K. Engineering a multi-biofunctional composite using poly(ethylenimine) decorated graphene oxide for bone tissue regeneration. *Nanoscale* **2016**, *8*, 6820−6836.
(54) Prins, H.-J.; Braat, A. K.; Gawlitta, D.; Dhert, W. J.; Egan, D. A.; Tijssen-Slump, E.; Yuan, H.; Coffer, P. J.; Rozemuller, H.; Martens, A. C. In vitro induction of alkaline phosphatase levels predicts in vivo bone forming capacity of human bone marrow stromal cells. *Stem Cell Res.* **2014**, *12*, 428−440.
(55) Diaz, L. A. C.; Elsawy, M.; Saiani, A.; Gough, J. E.; Miller, A. F. Osteogenic differentiation of human mesenchymal stem cells

DOI: 10.1021/acsomega.7b01139
ACS Omega 2017, 2, 5545−5556

promotes mineralization within a biodegradable peptide hydrogel. *J. Tissue Eng.* **2016**, *7*, No. 204173141664978.
(56) Keselowsky, B. G.; Collard, D. M.; García, A. J. Integrin binding specificity regulates biomaterial surface chemistry effects on cell differentiation. *Proc. Natl. Acad. Sci. U.S.A.* **2005**, *102*, 5953−5957.
(57) Rose, F. R. A. J.; Oreffo, R. O. C. Bone tissue engineering: hope vs hype. *Biochem. Biophys. Res. Commun.* **2002**, *292*, 1−7.
(58) Hummers, W. S., Jr.; Offeman, R. E. Preparation of graphitic oxide. *J. Am. Chem. Soc.* **1958**, *80*, 1339.
(59) Kumar, S.; Bose, S.; Chatterjee, K. Amine-functionalized multiwall carbon nanotubes impart osteoinductive and bactericidal properties in poly(ε-caprolactone) composites. *RSC Adv.* **2014**, *4*, 19086−19098.

DOI: 10.1021/acsomega.7b01139
ACS Omega 2017, 2, 5545−5556